Electronic Supplementary Information (ESI)

A High-Performance All-Metallocene-Based, Non-Aqueous Redox Flow Battery

Yu Ding, Yu Zhao, Yutao Li, John B. Goodenough and Guihua Yu*

Materials Science and Engineering Program and Department of Mechanical Engineering, The University of Texas at Austin, Austin, Texas 78712, USA.

Corresponding author email: ghyu@austin.utexas.edu

Experimental Details

Methods

Materials. Ferrocene ($FeCp_2$, 98%), ferrocenium hexafluorophosphate ($FeCp_2PF_6$, 97%), cobaltocene ($CoCp_2$), cobaltocenium hexafluorophosphate ($CoCp_2PF_6$), nickelocene ($NiCp_2$), bis(pentamethylcyclopentadienyl) cobalt ($CoCp_2$*), lithium hexafluorophosphate ($LiPF_6$, ≥99.99%), lithium bis(trifluoromethane) sulfonimide (LiTFSI, 99.95%), N,N-dimethylformamide (DMF, 99.8%) were purchased from Sigma Aldrich. Copper mesh (100 mesh, 99.6%), copper foil (30 μm thick, 99.5%), titanium foil (100 μm thick, 99.5%), polyvinylidene fluoride binder (PVDF), N-methyl-2-pyrolidone (NMP) and acetylene black were bought from Fisher Scientific. The NASICON-type $Li_{1+x+3z}Al_x(Ti,Ge)_{2-x}Si_{3z}P_{3-z}O_{12}$ (LATP) membrane was received from Ohara Corporation. The organic electrolyte (1 M $LiPF_6$ in ethylene carbonate/diethyl carbonate with volume ratio of 1:1), 1,3-dioxolane (DOL) and 1,2−dimethoxyethane (DME) were purchased from BASF.

Cell assembly. The static-mode half-cell assembly process is the same as our published paper and the static-mode full cell assembly process is similar with our previous report.[S1] Briefly speaking, Ti foil coated with acetylene black/PVDF works as current collector for both cathode and anode, and the battery module was built with LATP as separator sandwiched between two quartz shells. All the joints were sealed together with Surlyn® resin. Then the module will be transferred to glove box to inject electrolyte using syringe. The flow mode battery assembly process is almost the same, and the difference is that two modified cathode quartz shell with two hose barbs were used. Schematics of battery components, static mode battery and flow mode battery are shown in Fig. S1. In dQ/dV curves, the $FeCp_2$ based catholtye contains 0.1 M $FeCp_2$, 0.5 M $LiPF_6$ in DMA or DMF; or 0.1 M $FeCp_2$, 0.5 M LiTFSI in DOL or THF. The $CoCp_2$ based anolyte contains 0.1 M $CoCp_2$, 0.5 M $LiPF_6$ in DMA or DMF; or 0.1 M $CoCp_2$, 0.5 M LiTFSI in DOL or THF. The $CoCp'_2$ based anolyte contains 0.1 M $CoCp'_2$, 0.5 M LiTFSI in DOL. In half-cell test of $FeCp_2PF_6$, the catholyte is composed of 0.1 M $FeCp_2PF_6$, 0.5 M $LiPF_6$ in DMF; For $CoCp_2$, it is composed of 0.1 M $CoCp_2$, 0.5 M LiTFSI in DOL. In full-cell test, the catholyte is composed of 0.1 M $FeCp_2$, 0.1 M $FeCp_2PF_6$, 0.5 M $LiPF_6$ in DMF and the anolyte is composed of 0.1 M $CoCp_2$, 0.5 M LiTFSI in DOL. Different

concentrations of catholyte and anolyte were also prepared for comparison. The $CoCp'_2$ based anolyte contains 0.1 M $CoCp'_2$, 0.5 M LiTFSI in DOL. For RDE tests, 3 mM $FeCp_2$, 0.5 M $LiPF_6$ in DMF, 2.5 mM $CoCp_2$, 2.5 mM $CoCp_2PF_6$, 0.5 M LiTFSI in DOL/DME (volume ratio 1:1) were prepared separately.

Electrochemical characterization.

Galvanostatic charge/discharge tests were conducted on BioLogic VMP3 potentiostat system. RDE measurements were performed on BioLogic RRDE-3A rotating ring disk electrode with glassy carbon disk electrode. Specifically, the reference electrode is 0.01 M $AgNO_3$/0.1 M TBAP/CH_3CN, and the counter electrode is platinum electrode. Before all the RDE tests, the solutions were prepared in glove box and then sealed well. The scan rate was set at 5 mV s^{-1}, and the electrode was rotated at 100, 400, 900, 1600, 2500 and 3600 r.p.m. The limiting current versus the square root of the rotation rate is plotted, from which diffusion coefficient can be yielded. To fit the Koutecky-Levich equation, the reciprocal of the current at different overpotentials were plotted, and the intercept at the y axis gives the reciprocal of i_K at different overpotentials. By fitting Butler-Volmer equation, a linear plot of $\lg i_K$ versus overpotential can be got, and the yielded x-intercept is the log of the exchange current i_0. The rate constant of the redox reaction is proportional i_0 to according to the equation, $i_0=nFAk_0C$, from which we can get the reaction rate constant of 2.0×10^{-3} cm s^{-1} of $FeCp_2$, 5.3×10^{-4} cm s^{-1} of $CoCp_2$, and 1.7×10^{-3} cm s^{-1} of $NiCp_2$.

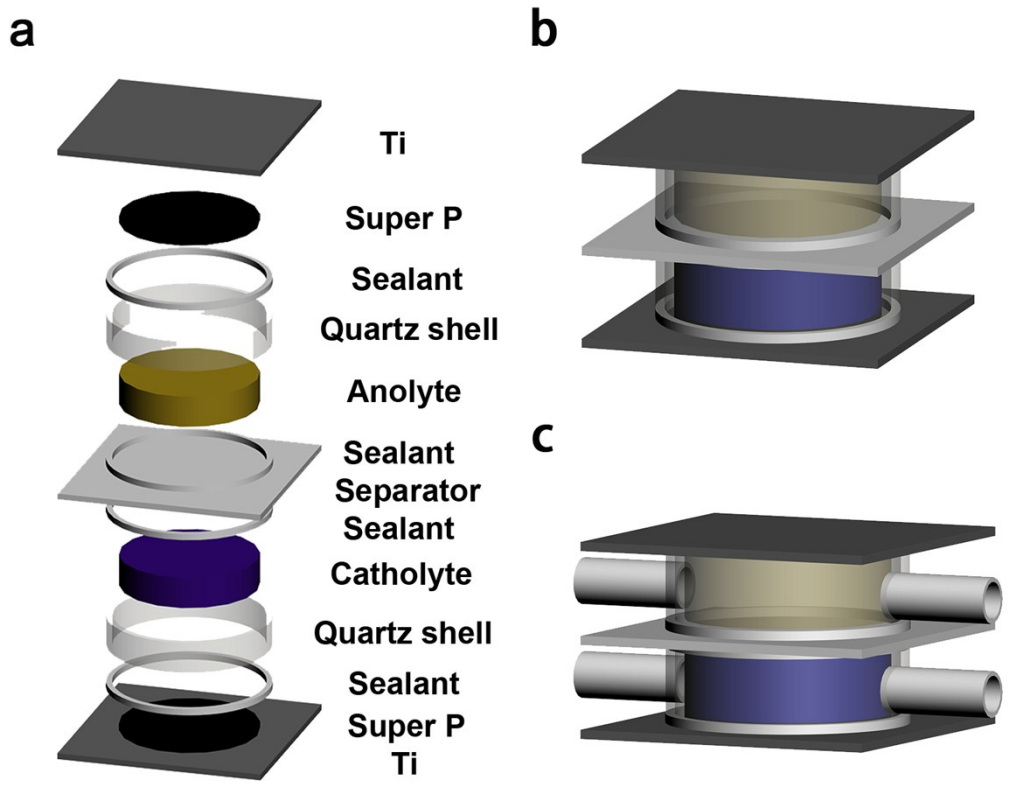

Fig. S1 (a) Cell components of static mode battery. (b) Schematic of a static mode liquid battery. (c) Schematic of a flow mode battery.

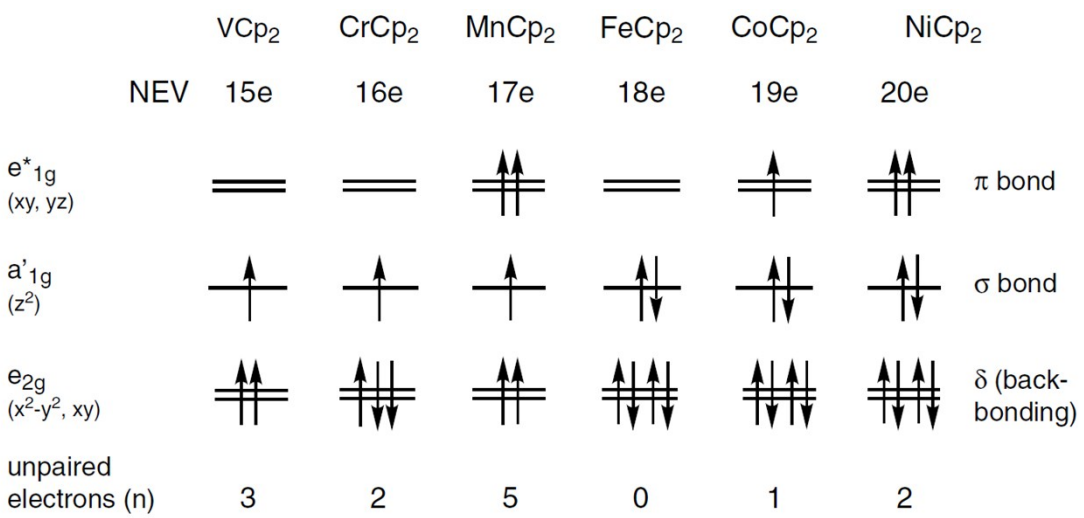

Fig. S2 Electronic structures of certain neutral metallocenes.

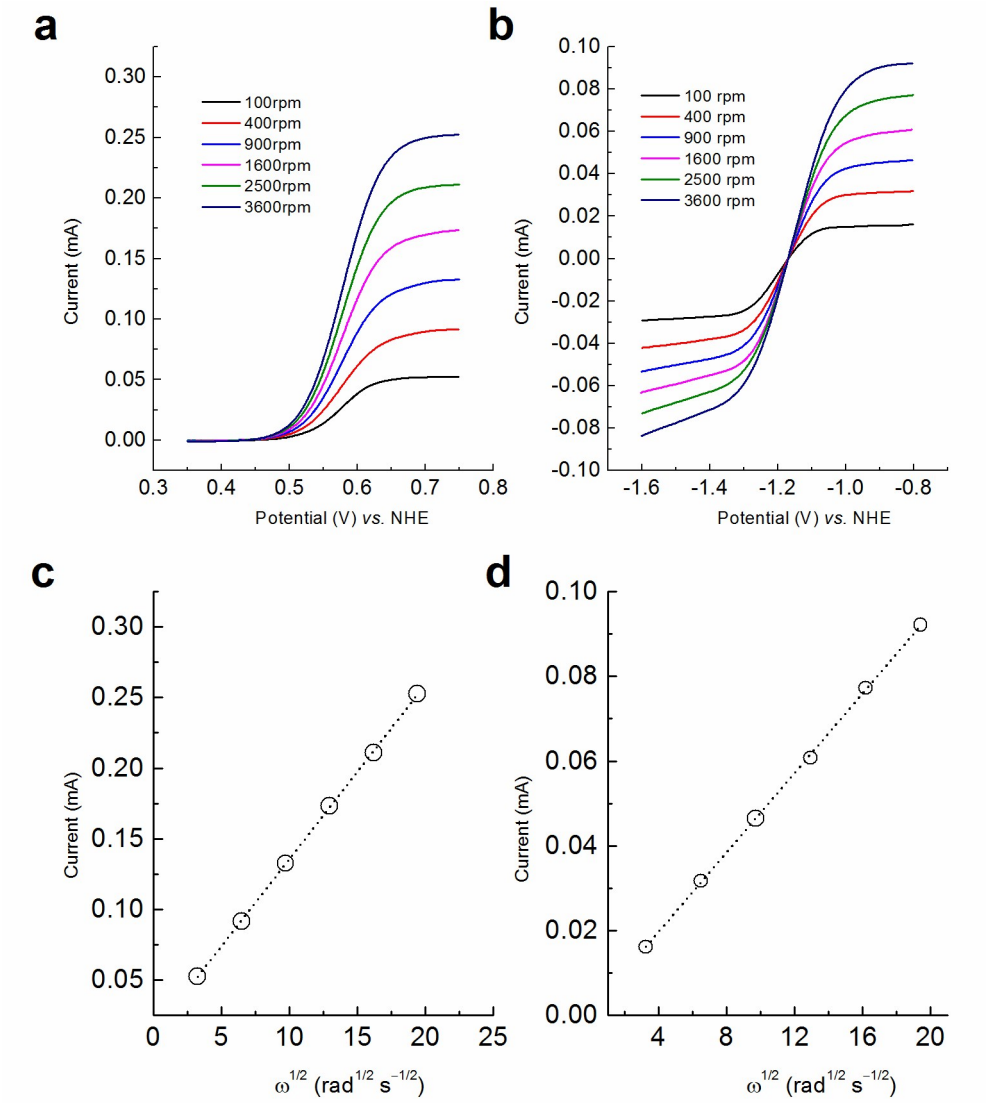

Fig. S3 RDE measurement of metallocenes. Voltammograms of metallocenes on glassy carbon electrode at six rotation speed ranging from 100 rpm to 3600 rpm with scan rate of 5 mV s^{-1}: (a) 3 mM $FeCp_2$, 0.5 M $LiPF_6$ in DMF. (b) 2.5 mM $CoCp_2$, 2.5 mM $CoCp_2PF_6$, 0.5 M LiTFSI in DOL/DME (volume ratio 1:1). Relationship between Levich current versus square root of rotation rate for metallocenes: (c) $FeCp_2$ and (d) $CoCp_2$.

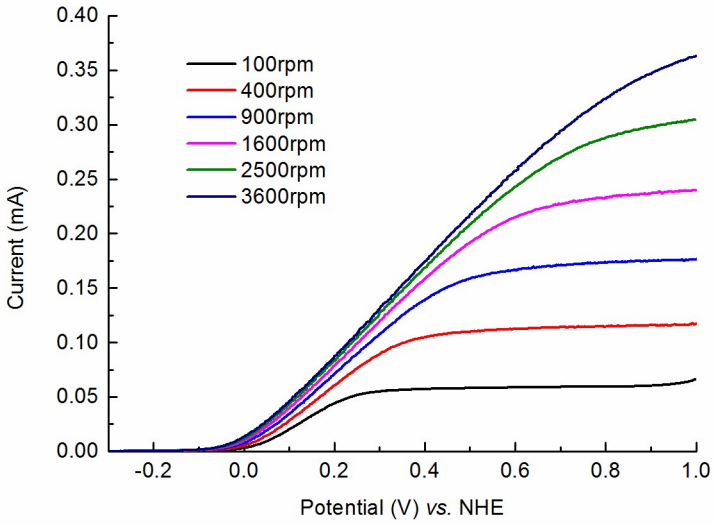

Fig. S4 Voltammograms of 3 mM $NiCp_2$, 0.5 M LiTFSI in DOL on glassy carbon electrode at six rotation speed ranging from 100 rpm to 3600 rpm with scan rate of 5 mV s^{-1}.

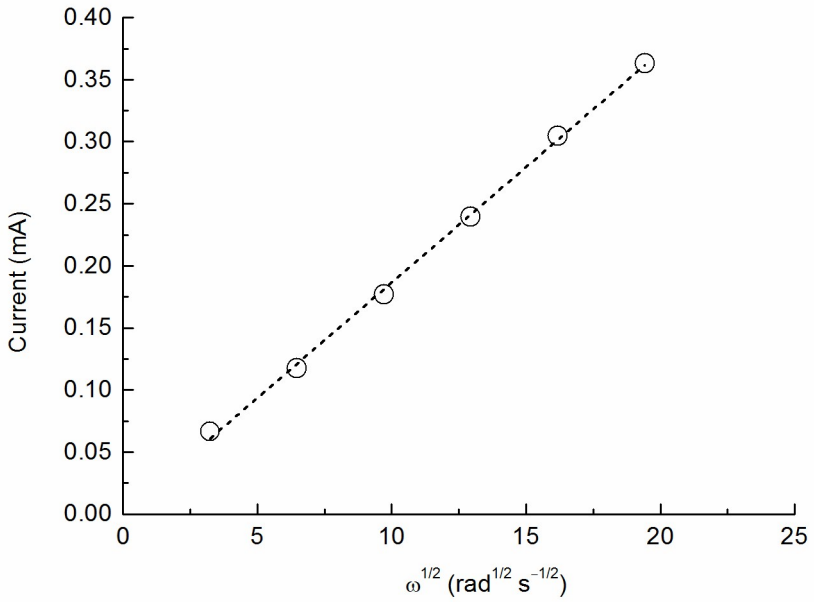

Fig. S5 Relationship between Levich current versus square root of rotation rate for $NiCp_2$.

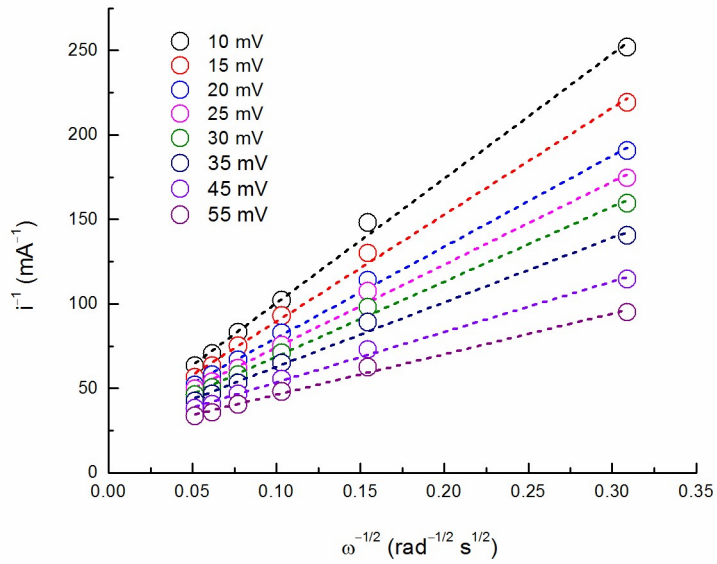

Fig. S6 Koutecky-Levich plots at different overpotentials derived from RDE test of $NiCp_2$.

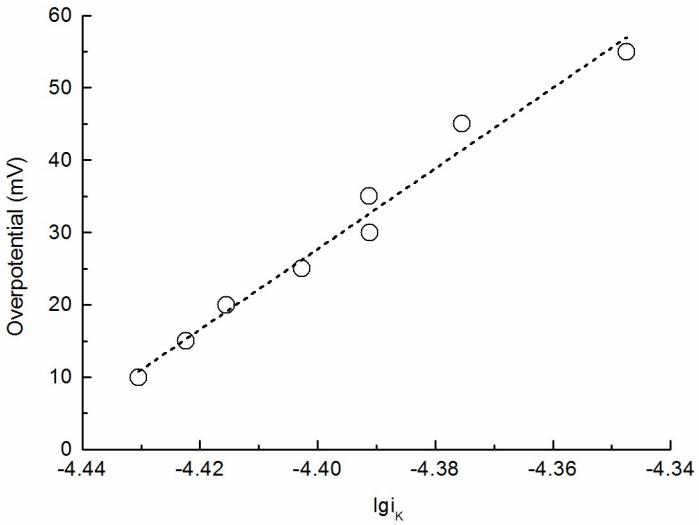

Fig. S7 Corresponding Butler-Volmer equation fitting of $NiCp_2$.

Table S1. Standard rate constants of redox species in commercial flow batteries.

Redox species	**Standard rate constant (cm s^{-1})**	**Electrode**
Fe^{3+}/Fe^{2+}	1.2×10^{-5}	Au (111)
Cr^{3+}/Cr^{2+}	2×10^{-4}	Hg
VO_2^{+}/VO^{2+}	3×10^{-7}	Graphite
Ce^{4+}/Ce^{3+}	1.6×10^{-3}	Pt
Br_2/Br^{-}	5.8×10^{-4}	Vitreous carbon

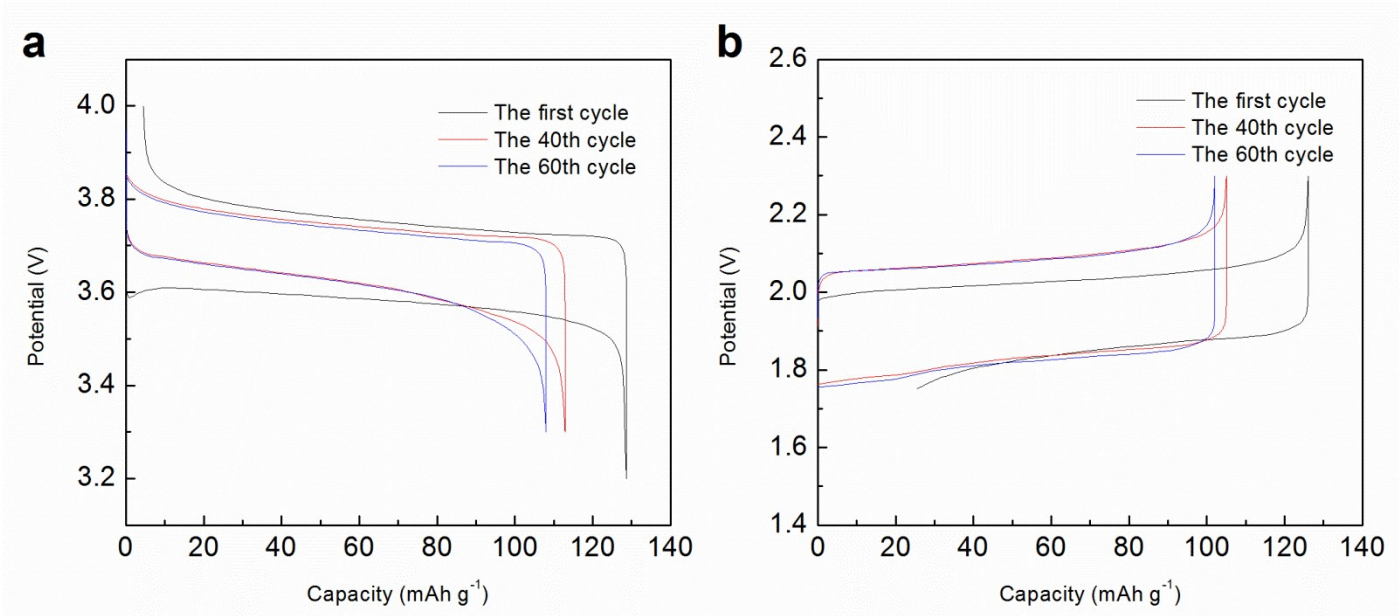

Fig. S8 Potential vs. specific capacity plot of the half battery at 0.4 C. (a) 0.1 M $FeCp_2PF_6$, 0.5 M $LiPF_6$ in DMF and (b) 0.1 M $CoCp_2$, 0.5 M LiTFSI in DOL.

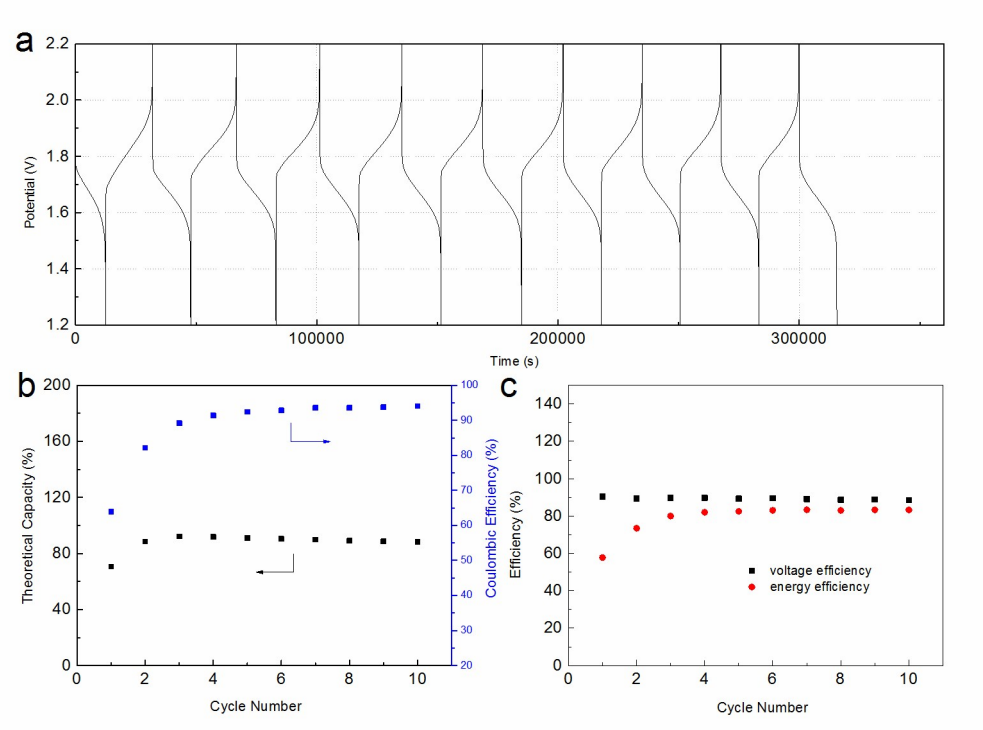

Fig. S9 Cyclic performance of the full battery using 0.1 M $FeCp_2$, 0.1 M $FeCp_2PF_6$, 0.5 M $LiPF_6$ in DMF on the positive side and 0.1 M $CoCp_2$, 0.5 M LiTFSI in DOL on the negative side at 0.4 C. (a) Potential vs. time plot. (b) Capacity, CE vs. cycle number. (c) Voltage and energy efficiency plot.

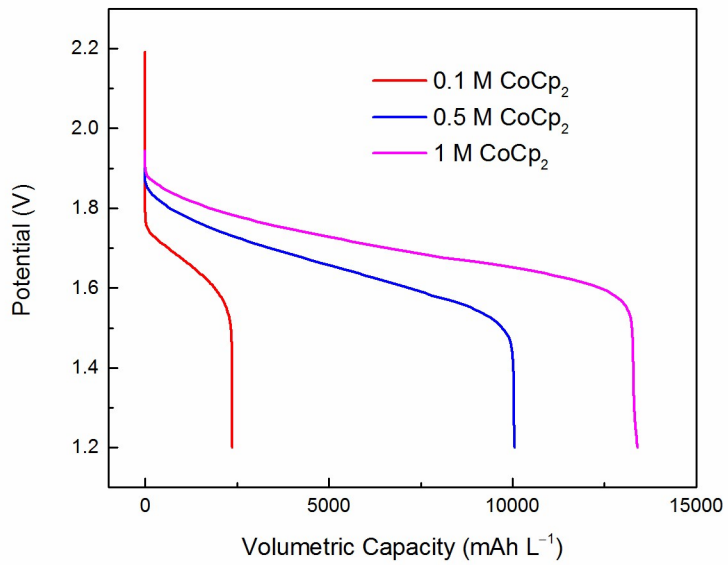

Fig. S10 Volumetric capacity of the full battery at 0.4 C for 0.1 M $CoCp_2$, 0.1 C for 0.5 M $CoCp_2$, and 0.05 C for 1 M $CoCp_2$.

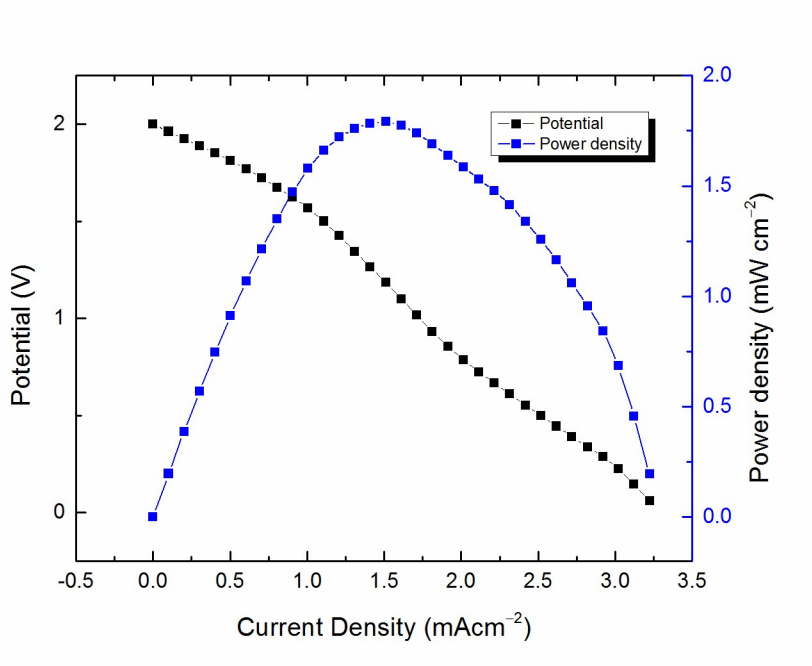

Fig. S11 Polarization curve for a flow mode battery using 0.1 M $FeCp_2$, 0.1 M $FeCp_2PF_6$, 0.5 M $LiPF_6$ in DMF on the positive side and 0.1 M $CoCp_2$, 0.5 M LiTFSI in DOL on the negative side.

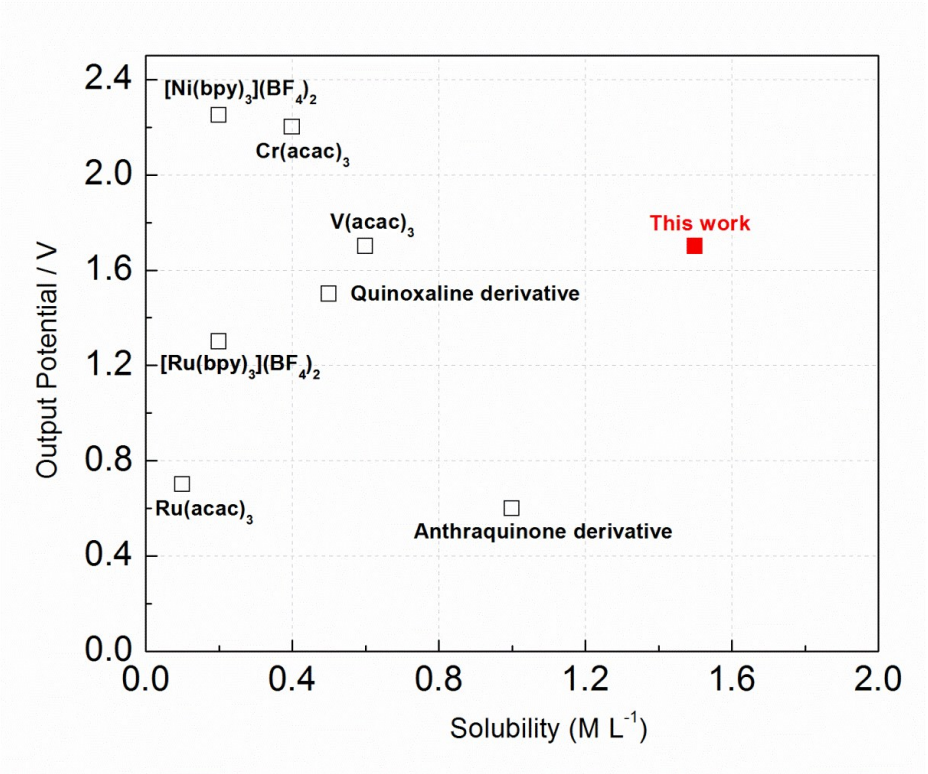

Fig. S12 Working potential versus solubility of anode-active material of recently developed redox flow battery.

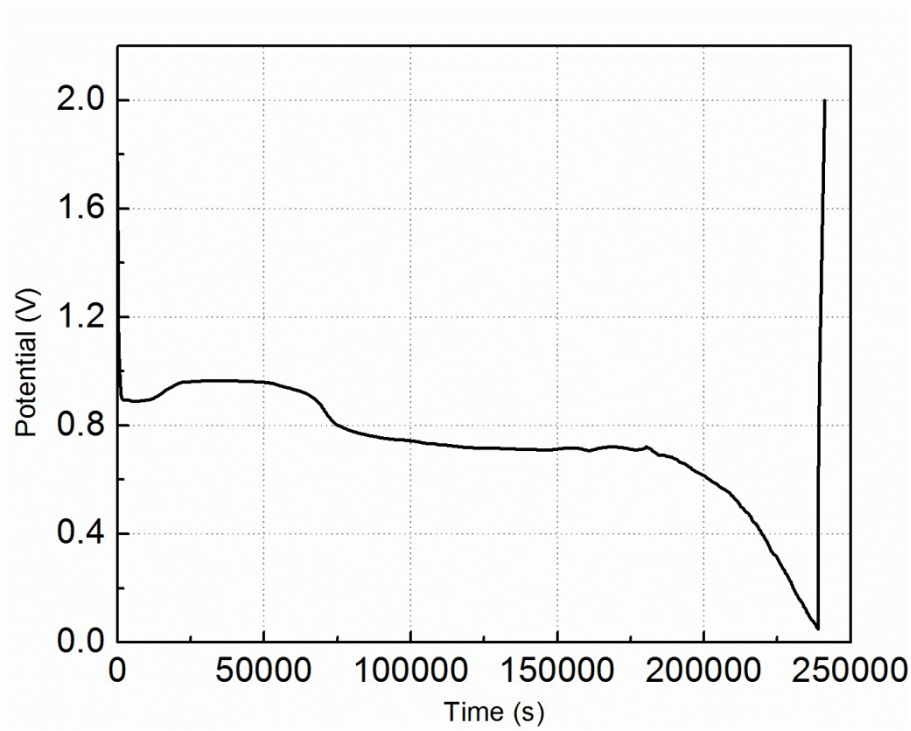

Fig. S13 Galvanostatic discharge-charge test of 0.1 M $CoCp_2$, 0.5 LiTFSI in DOL vs Li^+/Li between 0.05 V and 2 V at current density of 0.1 mA cm^{-2}.

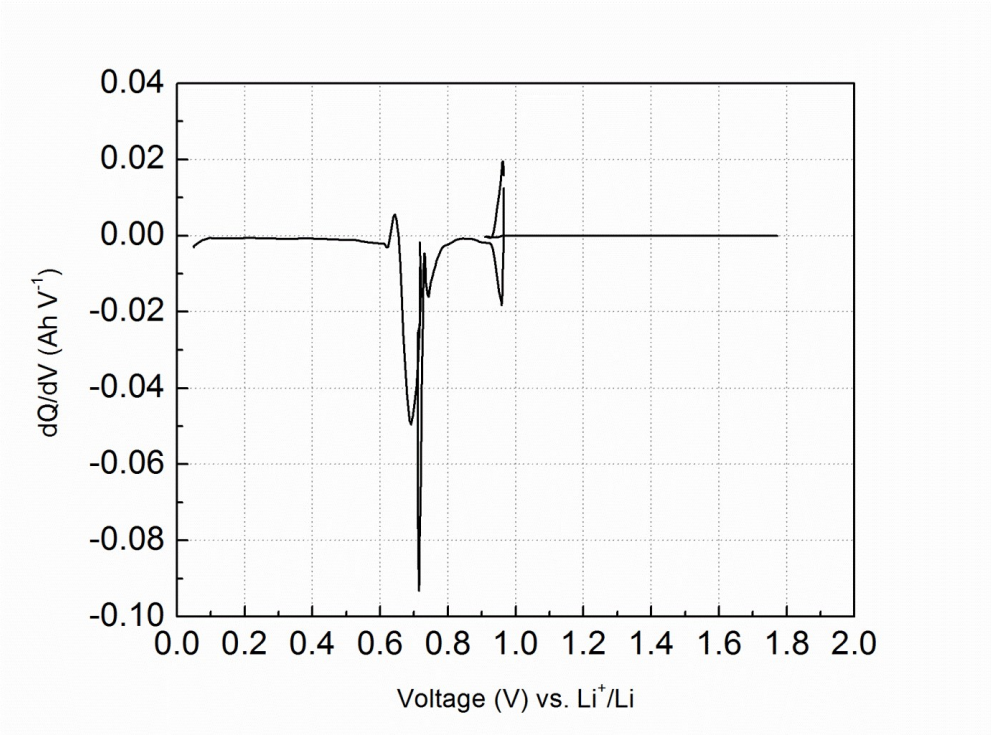

Fig. S14 dQ/dV vs. V curve of 0.1 M $CoCp_2$, 0.5 LiTFSI in DOL vs Li^+/Li between 0.05 V and 2 V at current density of 0.1 mA cm^{-2}.

References

S1. Y. Ding and G. Yu, *Angew. Chem. Int. Ed.*, 2016, **128**, 4850-4854.